We are IntechOpen, the world's leading publisher of Open Access books
Built by scientists, for scientists

6,000
Open access books available

147,000
International authors and editors

185M
Downloads

Our authors are among the

154
Countries delivered to

TOP 1%
most cited scientists

12.2%
Contributors from top 500 universities

CLARIVATE ANALYTICS
BOOK CITATION INDEX
INDEXED

WEB OF SCIENCE™

Selection of our books indexed in the Book Citation Index in Web of Science™ Core Collection (BKCI)

Interested in publishing with us?
Contact book.department@intechopen.com

Numbers displayed above are based on latest data collected.
For more information visit www.intechopen.com

Chapter

Aerodynamic Analysis and Performance Prediction of VAWT and HAWT Using CARDAAV and Qblade Computer Codes

Tayeb Brahimi and Ion Paraschivoiu

Abstract

Wind energy researchers have recently invited the scientific community to tackle three significant wind energy challenges to transform wind power into one of the more substantial, low-cost energy sources. The first challenge is to understand the physics behind wind energy resources better. The second challenge is to study and investigate the aerodynamics, structural, and dynamics of large-scale wind turbine machines. The third challenge is to enhance grid integration, network stability, and optimization. This chapter book attempts to tackle the second challenge by detailing the physics and mathematical modeling of wind turbine aerodynamic loads and the performance of horizontal and vertical axis wind turbines (HAWT & VAWT). This work underlines success in the development of the aerodynamic codes CARDAAV and Qbalde, with a focus on Blade Element Method (BEM) for studying the aerodynamic of wind turbines rotor blades, calculating the induced velocity fields, the aerodynamic normal and tangential forces, and the generated power as a function of a tip speed ration including dynamic stall and atmospheric turbulence. The codes have been successfully applied in HAWT and VAWT machines, and results show good agreement compared to experimental data. The strength of the BEM modeling lies in its simplicity and ability to include secondary effects and dynamic stall phenomena and require less computer time than vortex or CFD models. More work is now needed for the simulation of wind farms, the influence of the wake, the atmospheric wind flow, the structure and dynamics of large-scale machines, and the enhancement of energy capture, control, stability, optimization, and reliability.

Keywords: wind turbine, DMS, performance, loads, dynamic stall, induced velocity, power, normal and tangential forces

1. Introduction

Wind energy has been recognized as one of the fastest-growing energy sources in the world. The U.S. Energy Information Administration [1] reported that in 2020 the wind's annual electricity generation exceeds 300 million MWh in the U.S., which surpassed the hydroelectric generation by 26 million MWh. In the last decade, the global cumulative wind power capacity installed has increased from

about 200 gigawatts (GW) in 2010 to more than 650 GW in 2019, as shown in **Figure 1** [2, 3]. Compared to 2018, the global wind power installed capacity in 2019 represents a percentage increase of 19% with a 10% increase in new installation, which is the second-largest increase in the last decade. This increase was the result of the largest market from China (237029 MW), EU-28 (192231 MW), the USA (105433 MW), and India (37529) [3, 4]. With the continuous technology development of renewable energy, wind power becomes predominant than hydroelectric, biomass, or geothermal energy [5]. Currently, in Europe alone, electricity generated from wind turbines covers up to 11% of the electricity demand; by 2020, it will increase to 16.5%, and by 2030 it is expected that renewable energy could serve at least 27% of Europe electricity need, and will generate over three million jobs. Globally, in 2020 the anticipated wind energy will be dominated by China (38%), Europe (28%), US (16%), and India (7%) and by 2030, based on central scenario, it is expected to have a cumulative installation of 323 GW in Europe alone. Governments, policymakers, and energy utility companies currently employ a wide array of tools to encourage the deployment of various renewable energy technologies including investments, funds, cash, and tax credits incentives.

Before the COVID-19 pandemic, the Global Wind Report published by the Global Wind Energy Council expected a record of new wind installed capacity of 76.7 GW in 2020 [3]. However, given the unpredictable effects of COVID-19 on various renewable energy sectors, it is expected that the wind energy market will generally be slowing down, as the current control of the virus in the US, Europe, and China is still difficult to predict [2]. The International Energy Agency [6], in its new report on the market update outlook for 2020 and 2021, forecasts a 12% decrease in wind power growth compared to 2019. Statista, the online portal for statistics, reported that the global wind market is expected to add 73 gigawatts only instead of the previous predicted installed capacity of 76.7 [7]. The downturn is primarily attributed to project delays instead of cancelations. Yet, there is still a steady increase in global wind installed capacity; for example, the U.S. added 1821 megawatts (MW) of new installed capacity during 2020 Q1 [1], and India added 0.2 GW during January–March 2020 [8]. The International Energy Agency forecasts that over half of Europe's wind growth will come from the Netherlands, Germany, Sweden, Spain, and the U.K. There are currently up to 205 GW wind power installed capacity in Europe, representing 15% of EU-28 of the electricity consumed in 2019 [4].

With the growing ambition and enthusiasm on using the power of the wind to generate clean energy, added to the increasing investments and the drop in wind turbine pricing, more fundamental research and exploration is needed in the design of such wind turbine machines, including environment, social, and economic aspects of meeting the future functionality of large-scale deployment in both onshore and offshore areas. The present study aims to tackle one of the major problems that the wind turbine research community is concerned with [9, 10] by focusing on the aerodynamic loads and performance of vertical and horizontal performance wind turbines (VAWT & HAWT). The study provides a thorough mathematical and physics modeling of VAWT and HAWT aerodynamics using the Double-Multiple-Stream tube model (DMS) and blade element momentum theory (BEM) [11, 12].

2. Previous work

In the last few years, significant research activities have been devoted to designing large-scale wind turbines with high hub height and large rotor diameter, making

wind turbines the world's largest rotating machines. Wind turbine rotor diameters were in the range of 5 to 15 m during the 1980s, with an average capacity of 30 kilowatts. In the early 1990s, the wind turbine installed power reached 500 kW with a rotor diameter of 30 m. In 2000, the wind turbine installed power reached 1.0 MW with a rotor diameter of 50 m [13]. Since then, the size of wind turbines is getting larger and larger; in 2018, the power capacity increased to 2.6 MW with a diameter of 110 m, many wind farms have rotor diameters of up to 120 m 5-MW installed power. Current wind turbine technologies and advances in aerodynamics and structural analysis produce lighter and larger wind turbine machines with increased annual energy production [14]. Modern wind turbines may now reach 164 m of the rotor diameter and a power rating of 9.5 MW, such as the Vestas V164–9.5 MW. According to Statista [15], by 2021, the state-of-the-art wind turbine's rotor diameter is estimated to reach 220 meters. Recently, General Electric revealed the Haliade-X, the largest prototype ever designed by the company for a new offshore wind turbine and the most powerful wind turbine machine operating at a 13 MW power output and a rotor diameter of 220 m [16].

With the growing development of wind turbines on a large scale and the increasing amount of wind electricity generated, the current wind energy market needs to be a more competitive, cost-effective, and reliable renewable energy source. The International Renewable Energy Agency (IRENA) [13] reported several programs, projects, and research been introduced to investigate the development of such wind turbine machines and stimulate their commercial growth. The plans include innovation in rotor blade design and materials, optimization of power electronics, incorporating smart/intelligent wind turbines, and using recycling of materials the vast amount of materials used in the wind energy sector.

A long-term strategy to address the scientific and current wind turbine technology has been initiated by the European Academy of Wind Energy (EAWE) in 2016 [10]. The goal was to study and analyze the main barriers and priorities and promote cooperation among researchers in fundamental and applied sciences of wind turbines as more fundamental research and exploration are needed to design such large wind turbines. The EAWE presented and discussed 11 research challenges in wind energy development, namely the materials and structures, the wind and turbulence, the Aerodynamics of wind turbines, the control and system identification, the electricity conversion, the reliability and uncertainty modeling, the design methods, the hydrodynamics, the soil characteristics and floating turbines, the offshore environmental aspects, the wind energy in the electric power system, and the societal and economic factors of wind energy. Three years later, in the United States, the wind energy researchers [9] from the US Department of Energy at the National Renewable Energy Laboratory (NREL) invited the scientific community to interdisciplinary collaboration to tackle three significant wind energy challenges to transform wind engineering into one of the significant global low-cost power generation sources. The first grand challenge is to improve the understanding of the physics behind the wind resource and atmospheric flow in the critical region where the wind machine operates, the second big challenge is to tackle the corresponding structural and dynamics of large-scale rotating wind turbine machines, and the third grand challenge is the enhancement of energy capture, control, network stability, grid integration, optimization, and reliability. Nevertheless, to stay competitive, the cost of electricity generated from wind turbines must continue to decline.

Up to 75% of the overall costs of wind turbine energy production are attributed to upfront costs. In terms of the wind turbine machine's performance and cost, rotor blades are considered the most significant wind turbine parts. The aerodynamic design and optimum shape of the rotor blades, with a high lift to drag ratio, directly

impact the wind turbine performance and power generated. There are currently two types of modern wind turbine design: the Horizontal Axis Wind Turbine (HAWT) as the traditional wind pump, and the Vertical Axis Wind Turbine (VAWT) as the Darrieus design model. In both cases, the wind kinetic energy is extracted by the turbine's blades and transformed into electrical power. Both wind turbine machines are currently used offshore and onshore to generate electricity. Although the HAWT is widely used, the VAWT offers a promising alternative due to its mechanical and structural simplicity of harnessing wind energy, scaling down, safety and accepting wind flow from any direction. However, this simplicity encounters a significant challenge during the simulation and computation of the aerodynamic loads. Indeed, during each rotation, the rotor blades encounter the wake it generated, in addition to the wake generated by the rest of the blades, and operate in a dynamic stall regime [11, 17]. Adding to this is the fluctuating nature of the loads due to wind turbulence affecting the wind turbine's planned service life and the power generated, as reported in [18, 19].

Many aerodynamic models for predicting the forces and the power generated by a wind turbine have been developed. A complete state-of-the-art review, including the appropriate references, is given by [17, 20–25]. The wind turbine loads analysis can be achieved using three effective methods: the momentum method through Blade Element Momentum (BEM), the vortex theory, and the Computational Fluid Dynamics (CFD) method, and more recently using artificial intelligence (AI) to predict wind speed and power performance [26]. With the increased development and installation of wind turbines as wind farms, more work has been investigated in the wake velocity deficits generated by the upfront wind turbines. It has been reported that in a full-wake condition the wind turbine power loss may reach up to 40% [23]. The main objective of all the aerodynamic models is to first determine the induced velocity field generated in the upwind and downwind of the rotor blade where the flow through the wind turbine is considered to be subdivided into several streamtube. Then, the lift and drag coefficient as a function of the incidence angle needed to determine the normal, tangential forces as a function of the azimuth angle and, finally, the torque and the generated power. It is important here to note that the wind turbine performance is affected by many parameters such as wind speed, tip-speed ratio (TSR), airfoil shape and size, turbine aspect ratio (H/R), the solidity of the rotor, the swept area, the rotational speed, and other parameters such as dynamic stall effects, the presence of spoilers. Wind turbine aerodynamic loads and performance predictions in the vortex methods use lifting lines or surface to represent rotor blade trailing and shed vorticity in the wake then; the induced velocity is then determined at any point using the Biot-Savard law [21, 26]. Two types of vortex models have been used in this approach: the fixed-wake and the free-wake models. These vortex models need a significant amount of computer time to predict the aerodynamic loads and performance of the wind turbine machine more accurately than momentum models.

In the models using Navier–Stokes equations such as the case in a steady incompressible laminar flow using finite volume method based on the widely known "SIMPLER" algorithm [27], such models are well suited for wind farms as it can compute the flow velocity everywhere in the rotational plane of the wind turbine machine as well as in its vicinity. In a comparative study conducted by Perić et al. [28] using Blade Element Method and CFD on two types of wind turbines, the DTU 10 MW RWT (Denmark Technical University 10 MW Reference Wind Turbine) blade and the MEXICO blade (Model Rotor Experiments In Controlled Conditions), the authors predict the aerodynamic performance of with an accuracy of 15% accuracy for the 10 MW RWT blade and 6% accuracy for the MEXICO blade experiment data. The author recognizes the CFD's power to provide higher accuracy

compared to the BEM or vortex methods. While the BEM was limited to wind speeds of 10 to 12 m/s, the CFD method with $k - \omega$ turbulence model performed the prediction with wind speeds up to a range of 20 m/s. However, the authors indicated that the main disadvantage is the high computational time required for such analysis [28]. The present study will concentrate on the DMS method due to its simplicity, ability to include secondary effects, and, more importantly, the fast computation and run time compared to vortex or numerical models. This model can easily be applied to both VAWT and HAWT.

3. Double, multiple streamtube model (DMS), CARDAAV code

In the Double, Multiple Streamtube models (DMS) developed initially been by Paraschivoiu [11, 29], the variation in the upwind and downwind induced velocities as a function of the azimuthal angle has been included. In this case, the wind turbine blade is divided into several elements assuming no interaction between the components. This method's main principle is to determine the axial and angular induction factors using an iteration method. Then, the forces and power generated are defined in a similar manner to the VAWT. **Figure 1** shows the double streamtube model principle where the machine is represented by a pair of actuator disks in tandem in the upwind and downwind zone, CARDAAV Code. The induced velocity decreases in the axial direction so that the downwind induced velocity is smaller than the upwind zone. With $V_{\infty i}$ representing the local ambient wind velocity, V_e the equilibrium-induced velocity as shown in **Figure 1**, we can write the induced velocities as a function of the induced factor in the upwind zone named a and downwind zone named a'.

$$V = a\ V_{\infty i} \tag{1}$$

$$V_e = (2a - 1)V_{\infty i} \tag{2}$$

$$V' = a'V_e = a'(2a - 1)V_{\infty i} \tag{3}$$

$$V'' = (2a' - 1)(2a - 1)\ V_{\infty i} \tag{4}$$

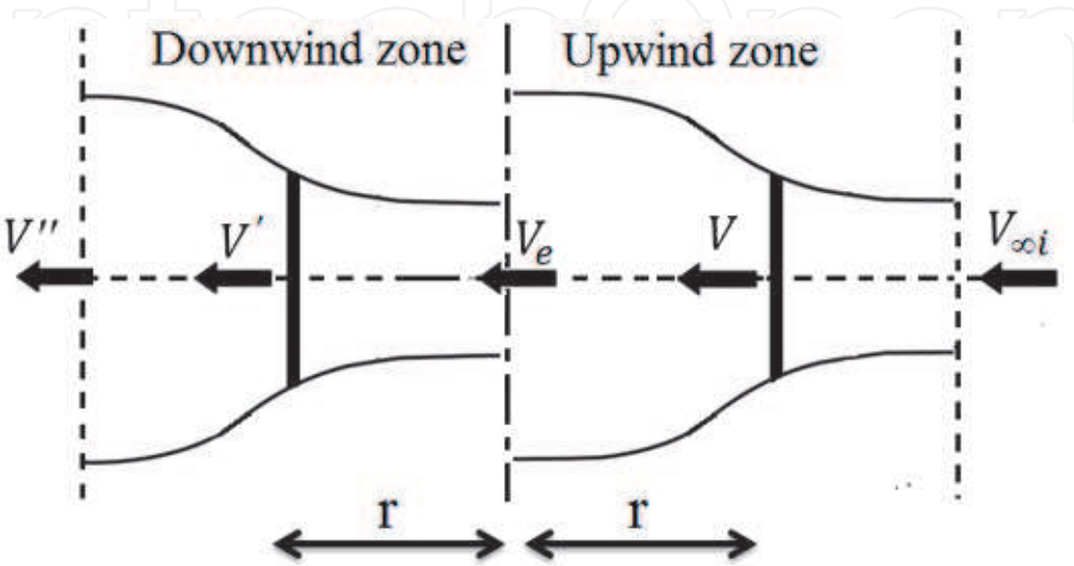

Figure 1.
Principle of the double multiple streamtube model.

The atmospheric wind shear in Eq. (5) is based on the Frost *et al.* model [30] where Z_{EQ} represents the height at the equator, $V_{\infty i}$ is the local ambient wind velocity in the vertical direction, V_∞ is the ambient wind velocity at the equator, and $\alpha_{\infty i}$is the exponent of the power-law, which in our simulation is taken to be 1/7.

$$\frac{V_{\infty i}}{V_\infty} = \left(\frac{Z_{\infty i}}{Z_{EQ}}\right)^{\alpha_{\infty i}} \tag{5}$$

The relative velocity and the local angle of attack in the upstream zone where the azimuth angle varies between $-\pi/2 \le \theta \le \pi/2$, are given by:

$$W^2 = V^2\left[(X - sin\theta)^2 + cos^2\theta cos^2\delta\right] \tag{6}$$

$$\alpha = arcsin\left[\frac{cos\theta cos\delta}{\sqrt{(X - sin\theta)^2 + cos^2\theta cos^2\delta]}}\right] \tag{7}$$

where $X = \omega r$ is the tip-speed ratio, and ω is the turbine rotational speed. For the downwind zone where the azimuth angle varies between $\pi/2 \le \theta \le 3\pi/2$ similar equations can be derived using W' and α'. The nondimensional normal and tangential forces as a function of the azimuth angle θ are given by

$$F_N(\theta) = \frac{c}{S}\int_{Z_R}^{Z_R+2H}\left(\frac{W}{V_\infty}\right)^2 C_N dZ \tag{8}$$

$$F_T(\theta) = \frac{c}{S}\int_{Z_R}^{Z_R+2H}\left(\frac{W}{V_\infty}\right)^2 \frac{C_T}{cos\delta} dZ \tag{9}$$

Using the same modeling above for the upwind region, the downwind area can also be calculated with the azimuth angle between $\pi/2 < \theta < 3\pi/2$. The normal and tangential force coefficients of the blade section are given by

$$C_N = C_L cos\alpha + C_D sin\alpha \tag{10}$$

$$C_T = C_L sin\alpha - C_D cos\alpha \tag{11}$$

where the lift and drag coefficients C_L and C_D are computed by interpolating the available test data using both the local Reynolds number $\left(R_e = \frac{Wc}{\mu_\infty}\right)$ and the local angle of attack. These coefficients are used up to an angle close to the static stall angle, from which point a dynamic-stall model is considered to estimate the dynamic lift and drag coefficients. The equations for the interference factor $a(\theta)$ are given by [11].

$$K[1 - a(\theta)]cos\theta = a(\theta)f(\theta) \tag{12}$$

$$f(\theta) = \left(\frac{W}{V}\right)^2\left[C_N cos\theta + C_T\left(\frac{sin\theta}{cos\delta}\right)\right] \tag{13}$$

where $K = \frac{8\pi r}{Nc}$ and N is the number of blades. The upwind half-cycle of the rotor is divided into several angular tubes $\Delta\theta$, assuming a constant induced velocity for each of these tubes, **Figure 2**. The interference factor $a(\theta)$ can be written as

$$a(\theta) = \frac{KK_0}{KK_0 + \int_{\theta-\frac{\Delta\theta}{2}}^{\theta+\frac{\Delta\theta}{2}} f(\theta)d\theta} \tag{14}$$

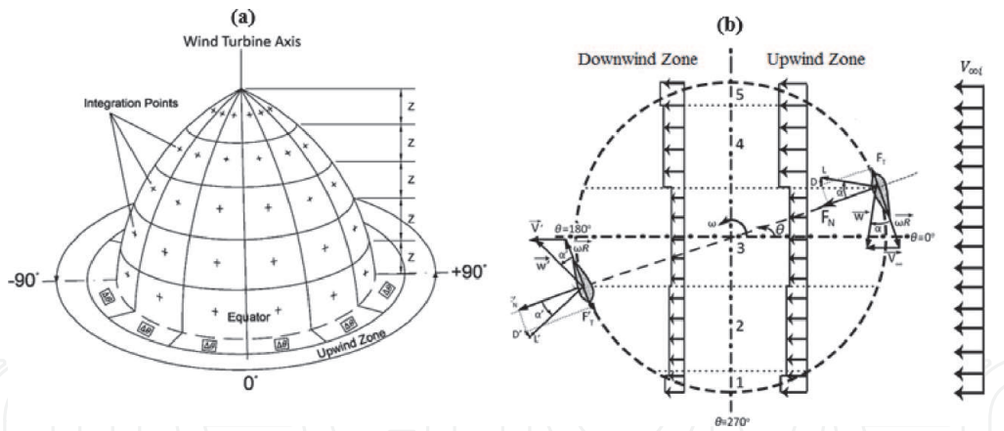

Figure 2.
VAWT model: (a) integration points, (b) DMS model.

where $K_0 = \sin\left(\theta + \frac{\Delta\theta}{2}\right) - \sin(\theta - \Delta\theta/2)$ and $a(\theta)$ is computed numerically. A similar technique is then used for the downwind zone to determine the interference factor $a'(\theta)$. The torque produced by the blade element as a function of the azimuth angle is calculated based on the lift and drag contributions C_{QL} and C_{QD}

$$C_{Q_L} = \frac{Nc}{2\pi SR}\int_{-\pi/2}^{3\pi/2}\int_{Z_R}^{Z_R+2H} C_L sin\alpha\left(\frac{W}{V_\infty}\right)^2 \times \left(\frac{r}{cos\delta}\right) dZd\theta \tag{15}$$

$$C_{Q_D} = \frac{Nc}{2\pi SR}\int_{-\pi/2}^{3\pi/2}\int_{Z_R}^{Z_R+2H} C_D cos\alpha\left(\frac{W}{V_\infty}\right)^2 \times \left(\frac{r}{cos\delta}\right) dZd\theta \tag{16}$$

Finally, the power generated due to the lift and the losses due to the drag is given by

$$P_L = \frac{1}{2}\rho_\infty V_\infty^3 S(C_Q)_L \frac{\omega R}{V_\infty} \text{ and } P_D = \frac{1}{2}\rho_\infty V_\infty^3 S(C_Q)_D \frac{\omega R}{V_\infty} \tag{17}$$

The impact of atmospheric wind turbulence on a wind turbine's aerodynamic loads can be included in the DMS model using a stochastic atmospheric wind. The induced velocities necessary for predicting the forces were computed for each Streamtube in both the upwind and downwind zones of the rotor, including the longitudinal and lateral fluctuation velocities resulting from the fluctuating atmospheric wind. A wind time series in the rotor's upwind zone is created to produce the turbulent wind velocity. Using a time delay in the time series based on a linear variation, the turbulent wind speed in the downwind zone is generated [11]. The total velocity of the fluctuating atmospheric wind is a superposition of a mean part and a stochastic fluctuating part. The values of the fluctuations velocities are performed by using the Fast Fourier Transform. The time series are assumed to propagate downstream of the rotor with the speed of the airflow disturbed by the presence of the wind turbine. The simulation uses Double-Multiple Streamtube model (DMS) with up to 1512 stream tubes for the whole Darrieus rotor (21 vertical stream tubes and 72 lateral stream tubes at every five degrees [11]. In the presence of atmospheric turbulence, the relative velocity and the local angle of attack are given by [18]:

$$W^2 = [(V + u_f)\sin\theta + v_f\cos\theta - \omega r]^2 + [v_f\sin\theta - (V + u_f)\cos\theta]^2\cos^2\delta \tag{18}$$

$$\alpha = \arcsin\left[\frac{v_f\sin\theta - (V + u_f)\cos\theta}{W}\right]\cos\delta \tag{19}$$

where V is the upwind velocity and u_f and v_f the fluctuation velocity components. The overall model developed "CARDAAS" performs the computation of steady-state, CARDAAV as well as the stochastic response of aerodynamic loads when turbulence is included [11, 18, 22].

4. QBlade aerodynamic code

Based on the Blade Element Momentum (BEM) method for the performance prediction of horizontal axis wind turbines (HAWT) and the Double Multiple Streamtube (DMS) method for the performance prediction of vertical axis wind turbine (VAWT), QBlade is an open-source used for wind turbine simulation and distributed under the General Public License with (GPL) free access [31–33]. The code includes extensive post-processing functionality for the rotor and wind turbine simulations, including different rotor blades and variables. The main modules of the QBlade computer code are given in **Table 1** [32]; the modules include the airfoil design, the viscous-inviscid coupled panel method XFOIL analysis, the airfoil polar extrapolation above the stall point, the HAWT and VAWT rotor blade design,

Module		Object
	Airfoil Design	Airfoil
	XFOIL Direct Analysis	Polar
	Polar Extrapolation to 360°	360° Polar
	HAWT Rotorblade Design	Blade
	Turbine BEM Simulation	Turbine
	QFEM - Structural Blade Design and Analysis	Structure
	FAST Simulation	FAST
	Turbulent Wind Field Generator	Wind Field

Table 1.
QBlade objects structure and modules.

the BEM simulation, the structural blade design and analysis, the simulation, and the turbulent wind field generator.

The theoretical formulation in QBlade is based on BEM and DMS. The rotor blade is discretized into a finite number of blade elements with defined cross-sections according to the radial position, profile, chord, twist, and length. Using the momentum theory, each blade section's relative wind speed is computed, which is then used to calculate the angle of attack and the Determination of the airfoil lift and drag coefficients. Once these parameters are known, the aerodynamic normal and tangential forces are computed, then the thrust and torque of an element are determined. Similar to CARDAAV code, in QBlade, the iteration variables of the BEM method are the two induction factors, axial a, and radial a' as shown in **Figure 3** where α is the angle of attack, $\varnothing$ is the inflow angle, θ is the pitch angle, and β is the twist angle. The wind velocity at the rotor blade is given by $V(1-a)$ in the horizontal direction, and the angular velocity is given by $\Omega r(1+a')$.

Based on **Figure 3**, the inflow angle $\varnothing$ and the relative velocity V_R are given by the equations

$$\varnothing = tan^{-1}\left[V_\infty \frac{1-a}{\Omega r(1+a')}\right] \tag{20}$$

$$V_R = V_\infty \frac{1-a}{sin\,\varnothing} \tag{21}$$

Using the momentum and BEM theory and the solidity $\sigma_r = \frac{Bc}{2\pi r}$ with B the number of blades and c the chord length, the axial and radial induction factors a and a' are computed from

$$a = \frac{1}{\frac{4\sin^2\varnothing}{\sigma_r C_N}+1} \text{ and } a' = \frac{1}{\frac{4\,sin\,\varnothing\,cos\,\varnothing}{\sigma_r C_T}-1} \tag{22}$$

where the normal and tangential force coefficients of the blade section are given by

$$C_N = C_L\,cos\,\varnothing + C_D\,sin\,\varnothing \tag{23}$$

$$C_T = C_L\,sin\,\varnothing - C_D\,cos\,\varnothing \tag{24}$$

The iteration technique used in the above equations is first to initialize the axial and radial induction factor a and a', then computer the inflow angle from Eq. (20),

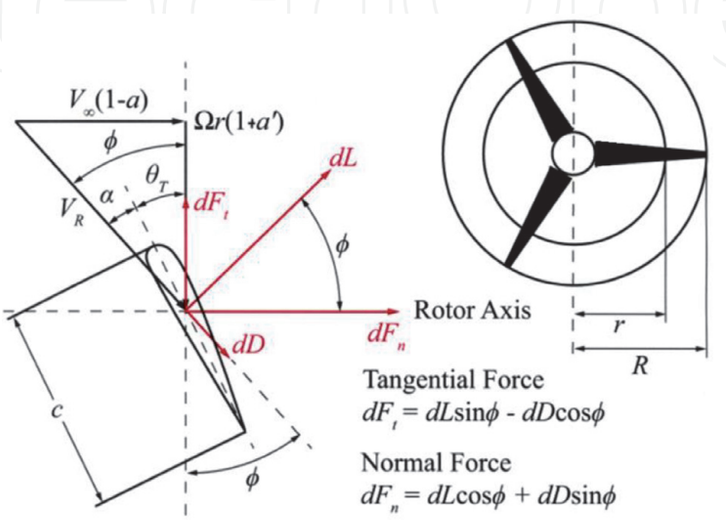

Figure 3.
Angles, velocity components, and forces acting on the HAWT rotor blade section.

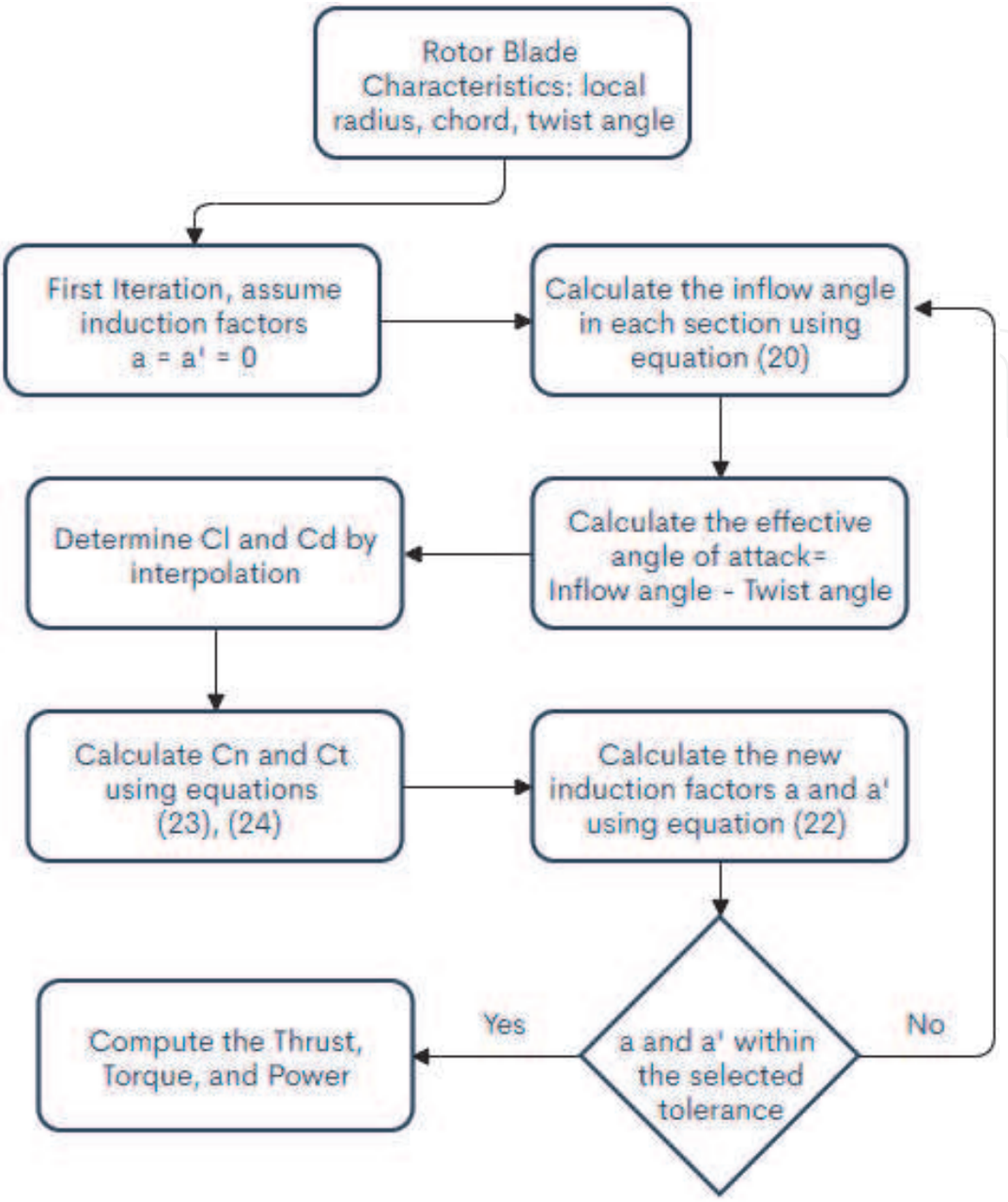

Figure 4.
Flowchart of the iterative algorithm used in QBlade.

the local angle of attack by subtracting the twist angle from inflow angle, use aerodynamic coefficients from tabulated airfoil data, compute a and a' from Eq. (22), compare the new axial and radial induction factors with the previous one, if not satisfied, return to step 2 by recalculating the inflow angle again in Eq. (20) and repeat the process if satisfied compute aerodynamic loads and performance of the wind turbine. For the vortices that form at the rotor's tip, resulting in added drag, the Prandtl tip loss factor is introduced [29, 33]. **Figure 4** shows a flowchart of the algorithm used in QBlade.

5. Secondary effects

The computer code CARDAAV can evaluate several rotor shapes with a straight or curved blade and use a defined shape such as a parabola, catenary, or modified troposkien. The code also can include the so-called "secondary" Effects," such as the

rotating tower, strut, and the spoiler. Another involved and unsteady phenomenon due to airfoil undergoing large and rapid variations of the angle of attack with time is the dynamic stall. During the rotor's rotation, the drag and lift coefficients present a different hysteresis than the case of static behavior. A dynamic delay of the stall to angles is substantially beyond the static stall angle, including massive recirculating regions moving downstream over the airfoil surface. In the case of VAWT, when the operational speed approaches its maximum, all the rotor blade sections go beyond the critical static stall angle of attack, the angle of attack changes substantially, and the entire blade operates under dynamic stall conditions, which will increase the unsteady blade loads and the wind machine structural fatigue. Different dynamic stall models with some modifications derived from static and dynamic airfoil tests have been incorporated into the CARDAAV computer code, such as the Gormont model and the indicial model [11, 34, 35]. Comparisons between aerodynamic performance predictions using dynamic-stall models show that the models provide a better prediction of the dynamic-stall regime characterized by a plateau oscillating near the experimental data of the rotor power function of wind speed [11].

6. Result and discussion

This section presents a selection of results obtained by performing aerodynamic loads and performance prediction using CARDAAV, different variants, and QBlade computer codes, including dynamic stall. Results were achieved on Sandia 17-m and 34 wind turbine machine [36] and compared to available experimental data. CARDAAV is the original code using an ambient constant ambient atmospheric wind speed, while CARDAAS code incorporated a stochastic wind to account for the atmospheric turbulence. Both CARDAAV and CARDAAS are based on DMS methods.

The viscous code 3DVF uses numerical methods to simulate the flow field of VAWTs in cylindrical coordinates based on the solution of steady, incompressible, and laminar Navier–Stokes equations. Different dynamic stall models have been incorporated into the aerodynamic codes, namely the original Gormont model, the

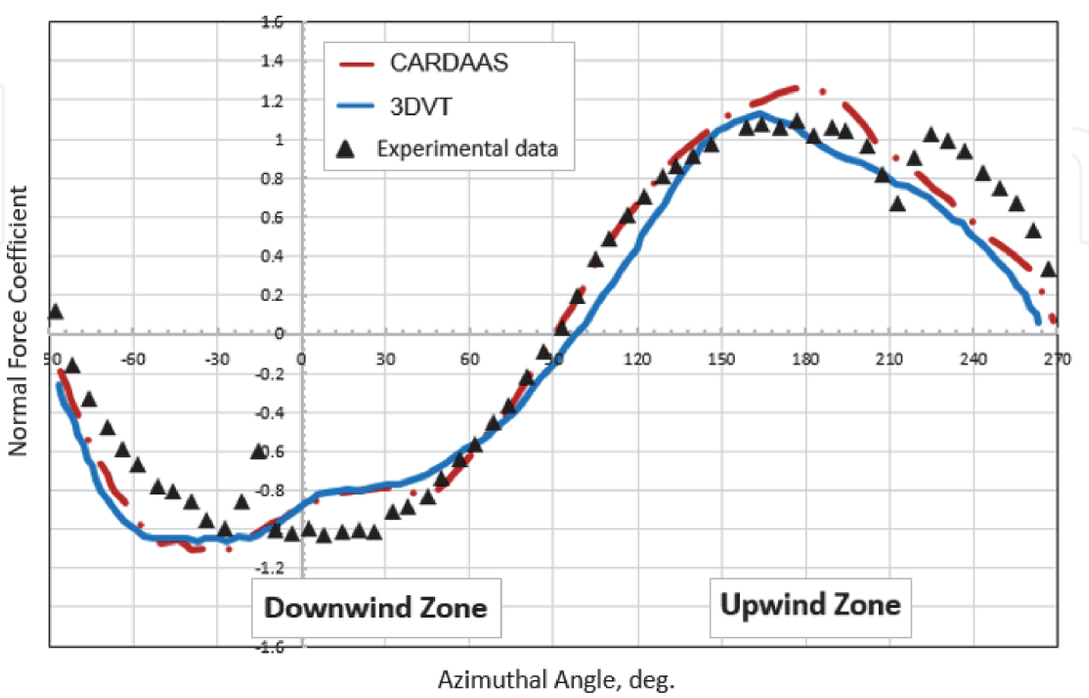

Figure 5.
Normal force coefficient as a function of azimuthal angle for 17-m wind turbine machine at TSR = 2.86.

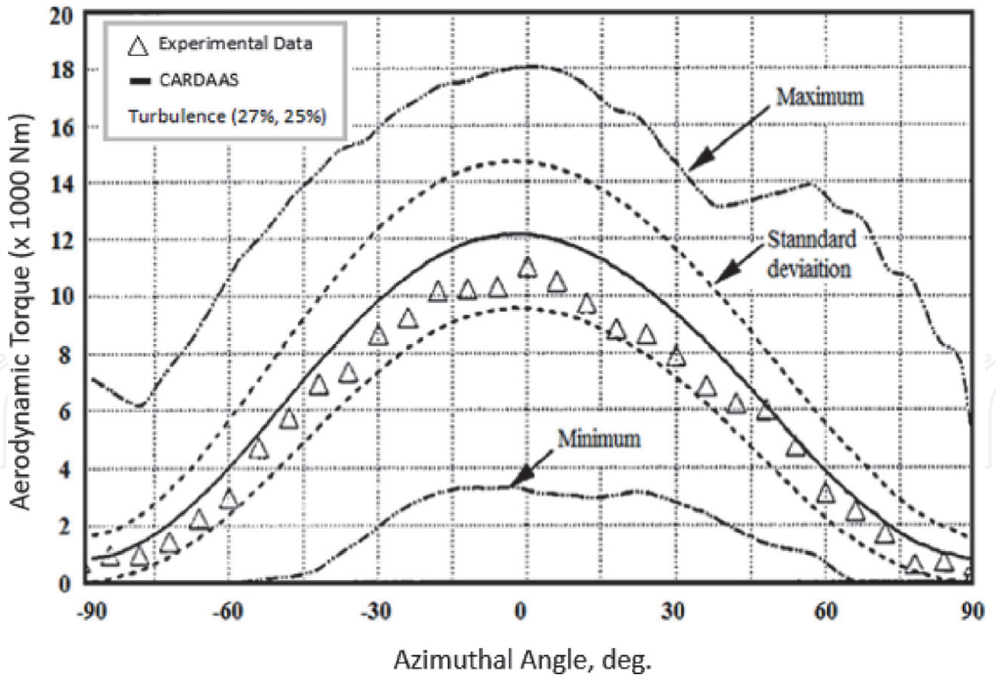

Figure 6.
Comparison of aerodynamic torque with experimental data at TSR = 4.60 and 50.6 rpm.

indicial model, and the MIT model [11, 34, 37]. **Figure 5** compares the normal force coefficient's distribution as a function of azimuthal angle for 17-m wind turbine machine at TSR = 2.86 using CARDAAS and 3DVF codes and experimental data. Using CARDAAS with low turbulence intensity induces a low variation in the ensemble-averaged values compared to the high turbulence intensity; obviously, for 0 turbulence intensity, both CRDAAV and CARDAAS give the same results. Comparing the two codes, one can conclude that CARDAAS and 3DVF predict quite well the distribution of the normal force coefficient. However, 3DVF is more time-consuming. **Figure 6** compares the normal force coefficient's distribution as a function of azimuthal angle for a 17-m wind turbine machine at TSR = 4.60 for a rotor rotation of 50.6 rpm. The distribution of the torque compares quite well with the experimental data. At the same time, it also gives the possibility to estimate the maximum and minimum torque encountered during the wind turbine rotation as a function of the azimuthal angle. **Figure 7** compares the wind turbine's theoretical performance with the experimental data for the Sandia 17-m turbine. The original CARDAA code does not include the variable interference factors used in CARDAAV code. As shown in this figure, CARDAA over predicts the power coefficient peak while CARDAAV shows a relatively good agreement with experimental data due to dynamic and secondary effects. Different dynamic stall models can be incorporated into the available aerodynamic codes. In **Figure 8**, the Gormont dynamic stall model and the improved Gormont model, along with the MIT dynamic stall models, have been used to predict the power generated by the wind turbine at different wind speeds.

All in all, the models forecast well the power generated by the wind turbine, but the early version of the Gormont over predict that power. In fact, the improved Gormont model by Paraschivoiu [11] takes into account the fact that high-level turbulence delays the onset of the dynamic stall. Based on that, the improved Gormont dynamic stall model is used at low turbulence zone only, namely between an azimuthal angle of 135 degrees and 15 degrees; the rest of the azimuthal angle will ignore the dynamic stall. In the MIT model case, the dynamic-stall regime is characterized by some variation compared to the improved Gormont model. In **Figure 9**, we present the case of the QBlade code used for HAWT and VAWT.

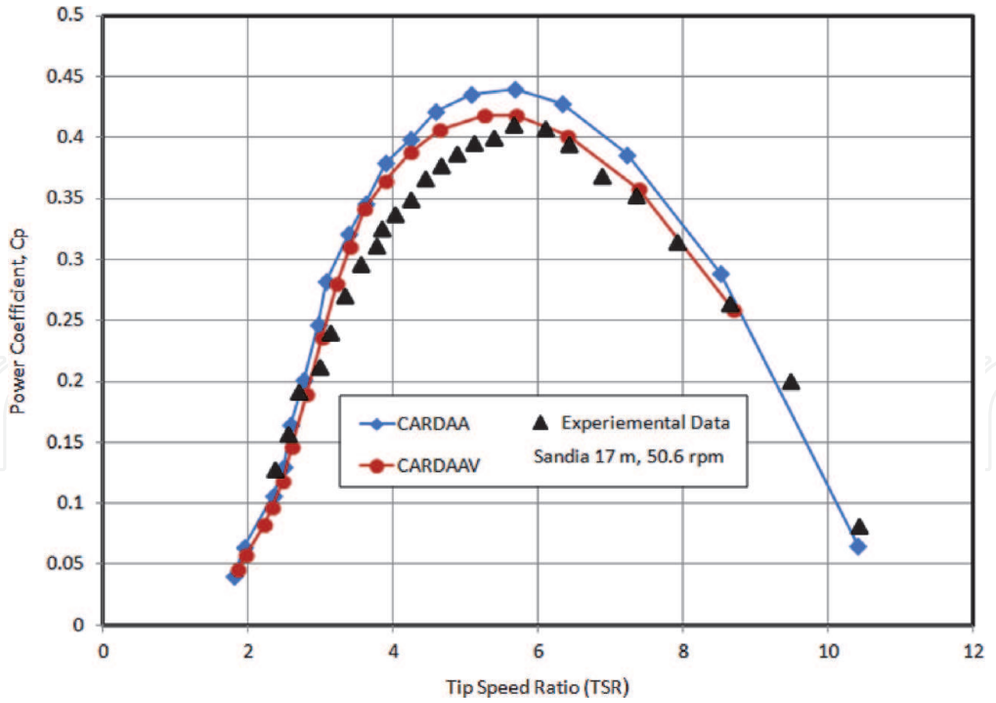

Figure 7.
Performance comparison between theoretical and experimental data for the Sandia 17-m turbine.

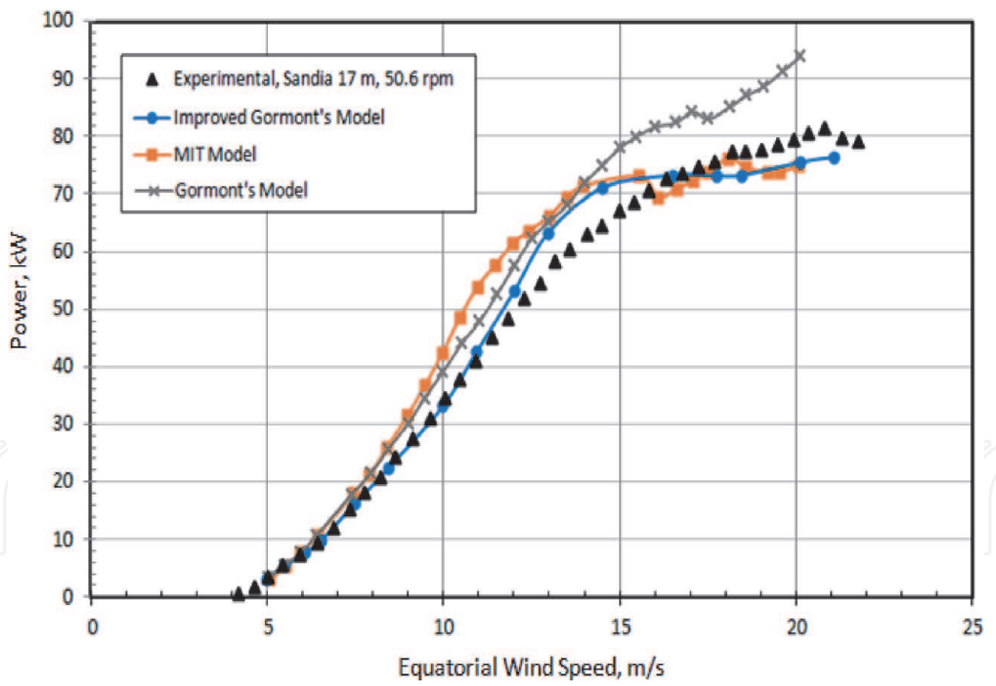

Figure 8.
Comparison of rotor power with different dynamic stall models at 50.6 rpm.

QBlade also uses the Blade Element Momentum (BEM) method and the DMS method to simulate HAWT and VAWT performance. Details on how to use QBlade can be found [31–33]. As an example, we generated the SG6043 airfoil pressure distribution generated using the XFOIL QBlade module. QBlade code can simulate the wake in the "Turbine Visualization" module, as shown in **Figure 10**. In **Figure 11**, we compare QBlade with CARDAAV code, including two dynamic stall models for the Sandia 34-m turbine, namely the indicial and improved Gormont models. The indicial model is used to simulate the effect of a dynamic stall at low

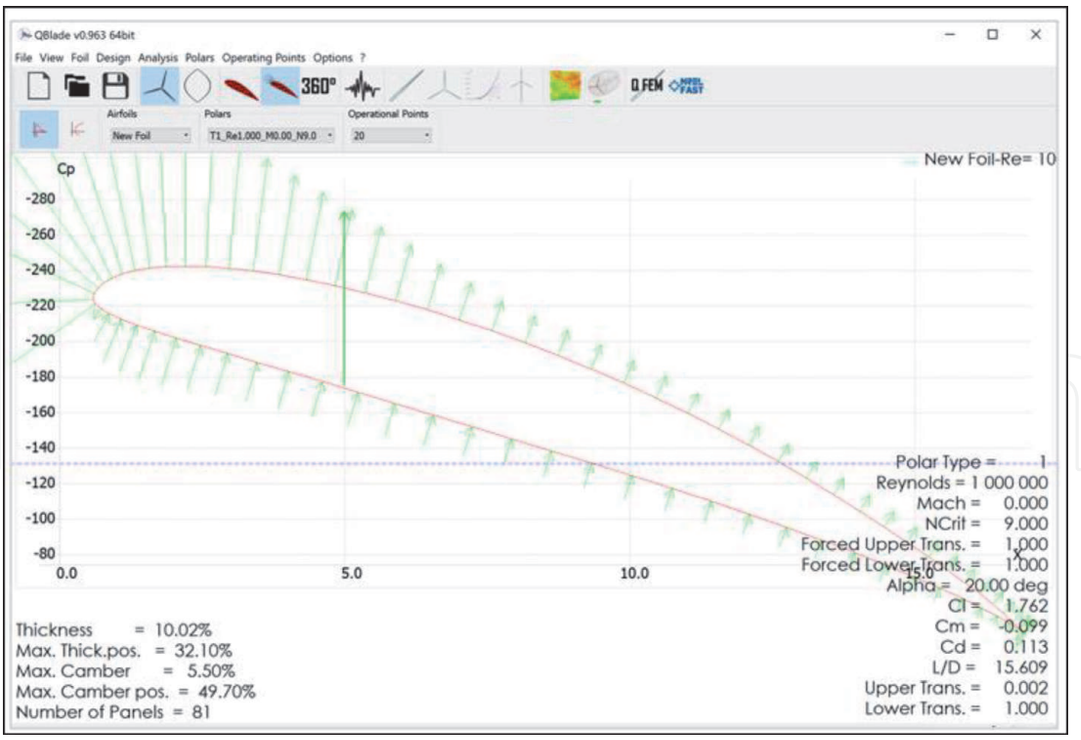

Figure 9.
Example of the SG6043 airfoil pressure distribution generated by QBlade.

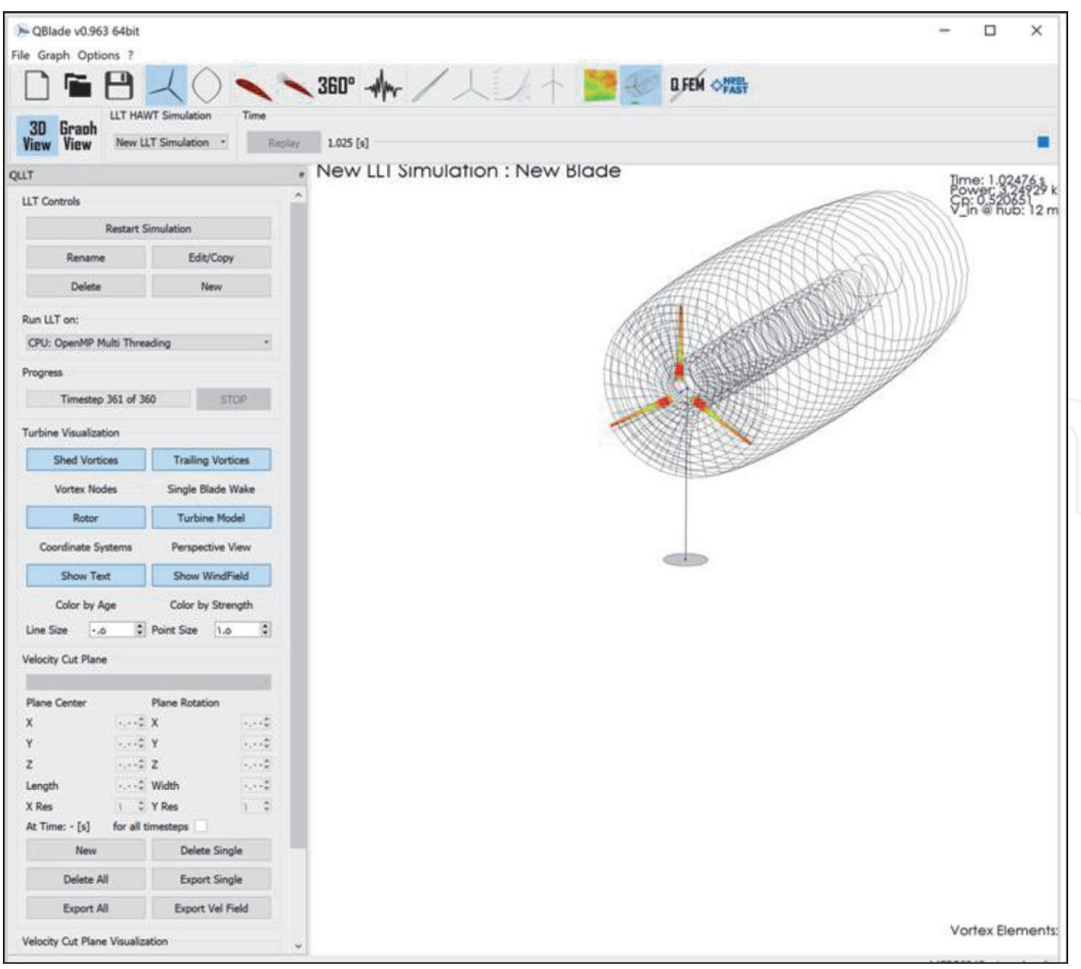

Figure 10.
Example of the wake simulation generated by QBlade.

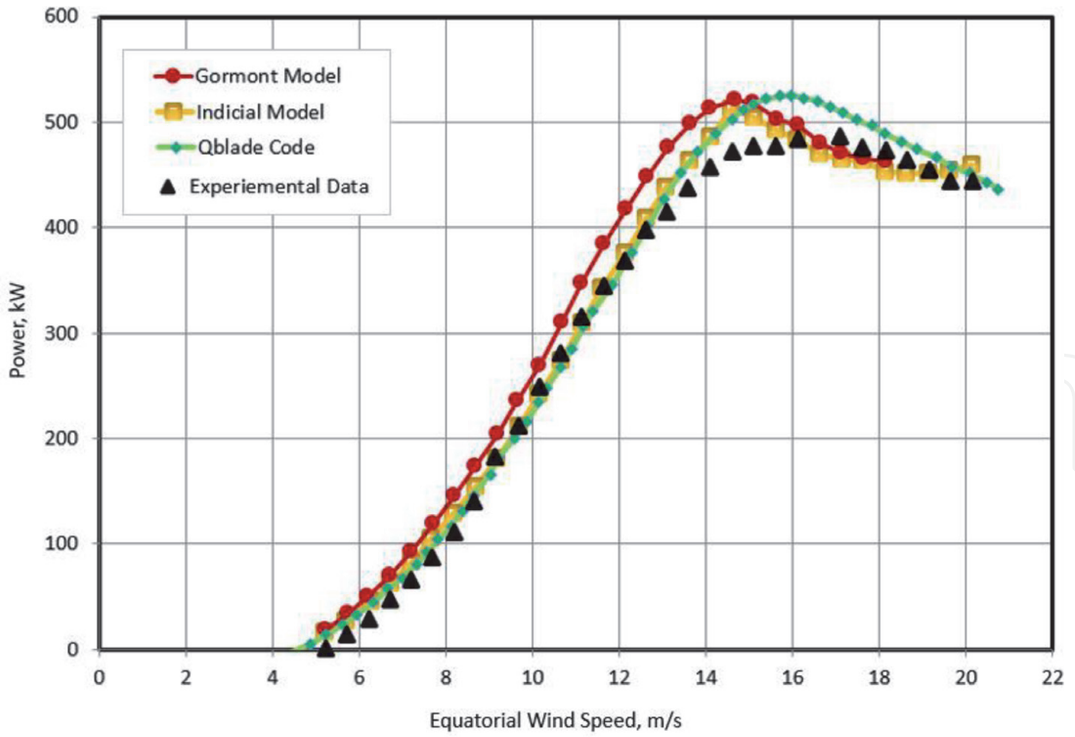

Figure 11.
Power distribution for the Sandia 34-m turbine using indicial and improved Gormont models at 34 rpm.

tip-speed ratios; it is basically centered on the fact the dynamic stall is considered to be a superposition of several different effects that can be independently explored by using indicial functions [34]. As shown by **Figure 11**, all models predict quite well the power generated by the wind turbine but QBLADE slightly over predicts the power compared to CARDAAV. More validation of the QBLADE code in the case of VAWT can be found in [38].

7. Conclusion

This book chapter emphasizes progress in the development of the aerodynamic codes for the prediction of HAWT and VAWT such as CARDAAV and Qbalde, with a focus on the BEMN and DMS methods for predicting aerodynamic and performance of wind turbines, including normal and tangential forces, torque, and the power generated by the wind turbine. The dynamic stall has been incorporated in this study to show the effects of this phenomenon on wind turbines' performance. The codes have been successfully applied compared to available experimental data for the 17 m and 34 m wind turbine machines. The strength of the available codes lies in their simplicity, fast prediction, and ability to include secondary effects. More work is now needed to simulate wind turbine wake and predict the performance of wind turbine farms, which requires the understanding of the physics of the atmospheric wind flow, the structure and dynamics of large-scale machines, and the enhancement of energy capture, control, stability, optimization, and reliability.

Acknowledgements

The authors gratefully acknowledge the support of the College of Engineering at Effat University, Jeddah, the Kingdom of Saudi Arabia, and the J.- Armand Bombardier Chair at Polytechnique of Montreal, Canada.

Author details

Tayeb Brahimi[1*] and Ion Paraschivoiu[2]

1 Energy Research Lab, College of Engineering, Natural Science, Mathematics and Technology Unit Effat University, Jeddah, Saudi Arabia

2 Department of Mechanical Engineering, Polytechnique Montreal, Montreal, PQ, Canada

*Address all correspondence to: tbrahimi@effatuniversity.edu.sa

IntechOpen

© 2021 The Author(s). Licensee IntechOpen. This chapter is distributed under the terms of the Creative Commons Attribution License (http://creativecommons.org/licenses/by/3.0), which permits unrestricted use, distribution, and reproduction in any medium, provided the original work is properly cited.

References

[1] AWEA. (2020, April 16). *American Wind Energy Association. Q1 2020 Installed Wind Power Capacity (MW)*. WINDExchange. https://windexchange.energy.gov/maps-data/321

[2] WWEA. (2020). World wind capacity at 650,8 GW, Corona crisis will slow down markets in 2020, renewables to be core of economic stimulus programmes. In *World Wind Energy Association*. https://wwindea.org/blog/category/statistics/

[3] GWEC. (2020). Global Wind Energy Report 2019. In *Global Wind Energy Council*. https://gwec.net/global-wind-report-2019/

[4] WindEurope. (2020). Wind energy in Europe in 2019 Trends and statistics. In *WindEurope*. Wind Europe. https://windeurope.org/about-wind/statistics/

[5] EIA. (2017). *Annual Energy Outlook 2017 with projections to 2050* (Report, U.S. Energy Information Administration #AEO2017; Annual Energy Outlook). U.S. Energy Information Administration. https://www.eia.gov/outlooks/aeo/

[6] IEA. (2020). *Renewable energy market update—IEA*. https://www.iea.org/reports/renewable-energy-market-update/covid-19-impact-on-renewable-energy-growth

[7] Sönnichsen, N. (2020). Covid-19 revised global wind energy additions forecast 2020. In *Statista*. https://www.statista.com/statistics/1107540/covid-19-global-wind-power-additions-forecast/

[8] Saurabh, A. (2020, May 23). *Nearly 85% Of Power Capacity Added in India in Q1 2020. Solar & Wind*. https://cleantechnica.com/2020/05/23/nearly-85-of-power-capacity-added-in-india-in-q1-2020-was-from-solar-wind/

[9] Veers, P., Dykes, K., Lantz, E., Barth, S., Bottasso, C. L., Carlson, O., Clifton, A., Green, J., Green, P., Holttinen, H., & al, et. (2019). Grand challenges in the science of wind energy. Science, *366* (6464). https://doi.org/10.1126/science.aau2027

[10] Kuik, G. A. M. V., Peinke, J., Nijssen, R., Lekou, D., Mann, J., Sørensen, J. N., Ferreira, C., Van Wingerden, J. W., Schlipf, D., Gebraad, P., & al, et. (2016). Long-term research challenges in wind energy – a research agenda by the European Academy of Wind Energy. *Wind Energy Science*, *1*(1), 1–39. https://doi.org/10.5194/wes-1-1-2016

[11] Paraschivoiu, Ion. (2009). *Wind turbine design: With emphasis on Darrieus concept*. Presses internationales Polytechniques.

[12] Sørensen, J. N. (2016). *General momentum theory for horizontal axis wind turbines*. Springer.

[13] *Deployment, investment, technology, grid integration and socio-economic aspects*. (n.d.). Retrieved January 16, 2021, from https://www.polity.org.za/article/deployment-investment-technology-grid-integration-and-socio-economic-aspects-2019-10-22

[14] Amano, R. S. (2017). Review of Wind Turbine Research in 21st Century. Journal of Energy Resources Technology, *139*(050801). https://doi.org/10.1115/1.4037757

[15] *Wind turbine rotor diameter size 2021.* (n.d.). Statista. Retrieved January 16, 2021, from https://www.statista.com/statistics/860565/global-rotor-diameter-size-of-wind-turbines/

[16] Reed, S. (2021, January 1). A Monster Wind Turbine Is Upending an Industry. *The New York Times*. https://

www.nytimes.com/2021/01/01/business/GE-wind-turbine.html

[17] Paraschivoiu, Ion, & Allet, A. (1988). Aerodynamic analysis of the Darrieus wind turbines including dynamic-stall effects. Journal of Propulsion and Power, *4*(5), 472–477. https://doi.org/10.2514/3.23090

[18] Brahimi, T., & Paraschivoiu, I. (1995). Darrieus Rotor Aerodynamics in Turbulent Wind. *1995*, *117*(2), 128–136. https://doi.org/10.1115/1.2870839

[19] Doubrawa, P., Barthelmier, R., Wang, H., & Chrchfield, M. (2016). A stochastic wind turbine wake model based on new metrics for wake characterization. WInd Energy, *20*(3). https://doi.org/10.1002/we.2015

[20] Branlard, E. (2017). The Blade Element Momentum (BEM) Method. In E. Branlard (Ed.), *Wind Turbine Aerodynamics and Vorticity-Based Methods: Fundamentals and Recent Applications* (pp. 181–211). Springer International Publishing. https://doi.org/10.1007/978-3-319-55164-7_10

[21] Hansen, M. O. L., Sørensen, J. N., Voutsinas, S., Sørensen, N., & Madsen, H. Aa. (2006). State of the art in wind turbine aerodynamics and aeroelasticity. Progress in Aerospace Sciences, *42*(4), 285–330. https://doi.org/10.1016/j.paerosci.2006.10.002

[22] Paraschivoiu, I., Saeed, F., & Desobry, V. (2002). Prediction Capabilities in Vertical-Axis Wind Turbine Aerodynamics. *, Berlin, Germany, 2–6 July 2002*.

[23] Sanderse, B., Pijl, S. P. van der, & Koren, B. (2011). Review of computational fluid dynamics for wind turbine wake aerodynamics. Wind Energy, *14*(7), 799–819. https://doi.org/10.1002/we.458

[24] Sørensen, Jens Nørkær. (2011). Aerodynamic Aspects of Wind Energy Conversion. Annual Review of Fluid Mechanics, *43*(1), 427–448. https://doi.org/10.1146/annurev-fluid-122109-160801

[25] Tristan, D., Turaj, A., & Joaquim, M. (2016). Aerodynamic shape optimization of wind turbine blades using a Reynolds-averaged Navier–Stokes model and an adjoint method. Wind Energy, *20*(5). https://doi.org/10.1002/we.2070

[26] Brahimi, T. (2019). Using Artificial Intelligence to Predict Wind Speed for Energy Application in Saudi Arabia. Energies, *12*(24), 4669. https://doi.org/10.3390/en12244669

[27] Allet, A., Brahimi, M. T., & Paraschivoiu, I. (1997). On the aerodynamic modelling of a VAWT. Wind Engineering, *21*(6), 351–365.

[28] Perić, B. M., Simonović, A. M., & Vorkapić, M. D. (2006). Comparative analysis of numerical computational techniques for Determination of the wind turbine aerodynamic performances. Thermal Science JOurnal, *2*. https://doi.org/10.2298/TSCI200216175P

[29] Hanson, M. O. L. (2008). *Aerodynamic of wind Turbines* (2nd ed.). Earthscan Publications Ltd.

[30] *NASA Technical Reports Server (NTRS)*. (n.d.). Retrieved January 18, 2021, from https://ntrs.nasa.gov/citations/19790006507

[31] Marten, D., Wendler, J., Pechlivanoglou, G., Nayeri, C. N., & Paschereit, C. O. (2013). QBlade: An open source tool for design and simulation of horizontal and vertical axis wind turbines. International Journal of Emerging Technology and Advanced Engineering, *3*(3), 264–269.

[32] *QBlade*. (n.d.). Retrieved January 18, 2021, from http://www.q-blade.de/

[33] HFI TU Berlin. (2013). QBlade Wind Turbine Design and Simulation. In *QBlade*. http://www.q-blade.org/

[34] Allet, A., & Paraschivoiu, I. (1995). *Viscous Flow and Dynamic Stall Effects on Vertical-Axis Wind Turbines*. International Journal of Rotating Machinery; Hindawi. https://doi.org/10.1155/S1023621X95000157

[35] Masson, C., Leclerc, C., & Paraschivoiu, I. (1998). *Appropriate Dynamic-Stall Models for Performance Predictions of VAWTs with NLF Blades*. International Journal of Rotating Machinery; Hindawi. https://doi.org/10.1155/S1023621X98000116

[36] Worstell, M. H. (1979). *Aerodynamic performance of the 17-metre-diameter Darrieus wind turbine* (SAND-78-1737). Sandia Labs., Albuquerque, NM (USA). https://www.osti.gov/biblio/6531371-aerodynamic-performance-metre-diameter-darrieus-wind-turbine

[37] Khan, M. A. (2018). *Dynamic Stall Modelling for Wind Turbines*. https://doi.org/10.13140/RG.2.2.26000.35848

[38] Marten, David, Lennie, M., Pechlivanoglou, G., Paschereit, C., Dy, N., Paraschivoiu, I., & Saeed, F. (2017). Validation and comparison of a newly developed aeroelastic design code for VAWT.